

# Elastocapillary Instability in Mitochondrial Fission

David Gonzalez-Rodriguez, Sébastien Sart, Avin Babataheri, David Tareste, Abdul I. Barakat, Christophe Clanet, Julien Husson

▶ **To cite this version:**

David Gonzalez-Rodriguez, Sébastien Sart, Avin Babataheri, David Tareste, Abdul I. Barakat, et al.. Elastocapillary Instability in Mitochondrial Fission. Physical Review Letters, 2015, 115 (8), pp.088102. 10.1103/PhysRevLett.115.088102 . hal-01207379

**HAL Id: hal-01207379**

**https://polytechnique.hal.science/hal-01207379**

Submitted on 30 Sep 2015

**HAL** is a multi-disciplinary open access archive for the deposit and dissemination of scientific research documents, whether they are published or not. The documents may come from teaching and research institutions in France or abroad, or from public or private research centers.

L'archive ouverte pluridisciplinaire **HAL**, est destinée au dépôt et à la diffusion de documents scientifiques de niveau recherche, publiés ou non, émanant des établissements d'enseignement et de recherche français ou étrangers, des laboratoires publics ou privés.

# Elastocapillary Instability in Mitochondrial Fission

David Gonzalez-Rodriguez,[1,*] Sébastien Sart,[1] Avin Babataheri,[1] David Tareste,[2] Abdul I. Barakat,[1] Christophe Clanet,[1] and Julien Husson[1,†]

[1]*Laboratoire d'Hydrodynamique, Ecole Polytechnique, CNRS UMR 7646, 91128 Palaiseau, France*

[2]*Institut Jacques Monod, Université Paris Diderot, INSERM U950, CNRS UMR 7592, 75205 Paris, France*

(Received 22 December 2014; revised manuscript received 3 June 2015; published 20 August 2015)

Mitochondria are dynamic cell organelles that constantly undergo fission and fusion events. These dynamical processes, which tightly regulate mitochondrial morphology, are essential for cell physiology. Here we propose an elastocapillary mechanical instability as a mechanism for mitochondrial fission. We experimentally induce mitochondrial fission by rupturing the cell's plasma membrane. We present a stability analysis that successfully explains the observed fission wavelength and the role of mitochondrial morphology in the occurrence of fission events. Our results show that the laws of fluid mechanics can describe mitochondrial morphology and dynamics.

DOI: 10.1103/PhysRevLett.115.088102 PACS numbers: 87.16.Tb, 47.20.Dr, 87.16.ad

Mitochondria are essential compartments of eukaryotic cells, since they supply energy, synthesize key molecules, and regulate calcium levels [1]. They consist of a double lipidic membrane surrounding a matrix. Mitochondria are typically tubular with submicrometric diameter and a length of several micrometers. However, this morphology is very dynamic, as mitochondria can undergo fusion and fission over time scales on the order of seconds to minutes [2]. Understanding the dynamics of mitochondrial morphology holds great importance in current biomedical research, since disruption of mitochondrial dynamics has been linked to neurodegeneration in Alzheimer's, Huntington's, and Parkinson's diseases [1]. Mitochondrial fission, i.e., the split of a mitochondrion into several smaller ones, is regulated by proteins of the dynamin superfamily, which form spirals around the outer mitochondrial membrane and sever it [3]. Significant mitochondrial fission is observed following stimuli that initiate apoptotic cell death [4]. Mitochondrial fission is also observed following pore formation in the cell's plasma membrane induced by bacterial infection [5]. In the latter case, the mitochondrial fission mechanism remains unknown, as such fission events do not require the canonical fission machinery regulated by dynamin-like proteins [6].

In this Letter, we propose that mitochondrial fission can be induced by a mechanical instability. To study mitochondrial fission following the loss of integrity of the cell's plasma membrane, of relevance to understanding bacterial-induced mitochondrial fission, we developed the experimental setup illustrated in Fig. 1. A detailed description of the experimental protocol is provided in the Supplemental Material [7]. Briefly, primary bovine aortic endothelial cells were plated at a subconfluent density on a glass-bottom dish. Before experiments, cells were incubated with the mitochondrial fluorescent probe MitoTracker. We used a glass micropipette to impact and locally rupture the cell's plasma membrane. The micropipette body was bent to a 45° angle, so that its tip could be positioned perpendicular to the plane where the endothelial cells adhered (see the inset in Fig. 1). The setup was mounted on an inverted microscope equipped with a 100× objective. Experiments were performed at 37 °C using a heating stage on the microscope. Time lapse movies were acquired at a rate of 2 frames per second, with a 200 ms exposure time.

A typical time evolution of mitochondrial morphology following plasma membrane disruption is shown in Fig. 2 (see also Movie 1 in the Supplemental Material). The inset shows how mitochondria, which initially have a tubular shape, may fission into smaller fragments, which then

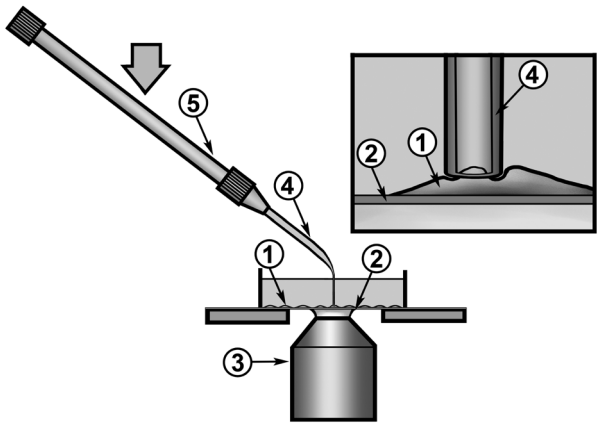



FIG. 1. Sketch of the experimental setup. (1) A layer of bovine endothelial cells (represented by the undulated curve) is grown on (2) a glass-bottom dish. The dish is filled with culture medium and placed on (3) an inverted microscope. (4) A curved glass micropipette, manipulated by means of (5) a micropipette holder, is used to exert a controlled impact on the cell's plasma membrane (indicated by the block arrow) and to rupture it. The inset represents the contact between the micropipette tip and the cell.

 © 2015 American Physical Society

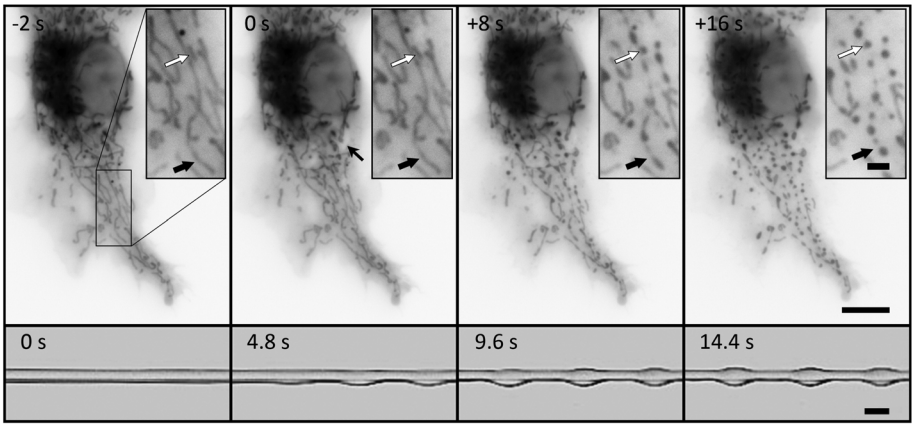



FIG. 2. Top row: Time sequence of the morphological change of mitochondria (fluorescently labeled in black), following the micropipette-induced plasma membrane rupture that occurs at time $t = 0$ s and at the location indicated by the left-pointing black arrow. The scale bar measures 10 $\mu$m. The inset shows a magnification of the mitochondrial morphological change. The black arrow in the inset follows an unstable mitochondrion, and the white arrow follows a stable one. The inset's scale bar measures 2 $\mu$m. Bottom row: Time sequence of the Plateau-Rayleigh instability of a water film on a glass fiber. The scale bar measures 1 mm.

become round over a typical time on the order of 15 s. As seen in the inset, longer mitochondria tend to fission into several fragments (right-pointing black arrows in Fig. 2), whereas shorter mitochondria tend not to fission but to simply become round following plasma membrane disruption (white arrows in Fig. 2). Such mitochondrial fission events require the plasma membrane to be disrupted, which can be attained by a mechanical shock or by other means, such as a hypotonic osmotic shock or saponin-induced plasma membrane permeabilization (see the Supplemental Material).

The observed mitochondrial fission resembles the classic capillary instability of a liquid cylinder, first described by Plateau [12] and Rayleigh [13] and illustrated in the snapshots in the bottom row of Fig. 2. An analogy with the Plateau-Rayleigh instability has previously been exploited to explain the emergence of "pearling" states in lipid tubes [14] as well as pattern development during the growth of biological tubes [15]. Similar to these previous studies, we assume that the mitochondrial mechanics are characterized by a membrane tension $\gamma$ and by a mechanical resistance to deformation. In the pearling instability of lipid tubes described in Ref. [14], the dominant resistance to deformation is the bending rigidity of the lipid membrane. In mitochondria, this bending resistance scales as $B/R_0^2 \approx 10^{-6}$ J/m$^2$, where $B \approx 5 \times 10^{-20}$ J is the bending modulus of a lipid membrane and $R_0 \approx 200$ nm is the typical undeformed mitochondrial radius. This bending resistance is 1 order of magnitude smaller than the typical mitochondrial membrane tension, which tends to round the mitochondrion and has previously been reported to be of the order of $\gamma \approx 10^{-5}$ J/m$^2$ [16]. Unperturbed mitochondria remain tubular, and thus they must possess an additional resistance to deformation, which we represent by an effective elastic modulus $E$. We propose that this dominant elastic resistance arises from the mitochondrial inner membrane folds, known as cristae. Cristae have been observed to connect to each other [17], thus forming a three-dimensional network that resists deformation. The structure of this network is, however, very sensitive to biochemical perturbations [17], which can reorganize the cristae and thus alter the value of $E$.

In the mechanical picture we propose, mitochondrial shape depends on the ratio between $E$ and $\gamma$, which is a form of the elastocapillary number [18], here defined as $N_{\mathrm{EC}} \equiv Ed_0/\gamma$, where $d_0$ is the membrane thickness. In the tubular configuration, $N_{\mathrm{EC}} > 1$ and the cylindrical shape is stable. However, upon rupture of the cell's plasma membrane, mitochondrial mechanical properties change so that $N_{\mathrm{EC}}$ decreases, yielding a morphological change towards the spherical shape. The molecular processes inducing this mechanical change remain to be determined. A first candidate process is a pressure increase inside the mitochondrion, which would increase $\gamma$. Indeed, repeating our experiments in hypertonic conditions (which induce mitochondrion shrinking and a reduction of $\gamma$) results in a decreased incidence of mitochondrial fission, whereas hypotonic conditions have the opposite effect (see the Supplemental Material). A second candidate process is a change in the transmembrane potential across the inner mitochondrial membrane, which has been correlated to changes in the inner membrane topology [19] and in its elastic properties [20], thus reducing $E$. Indeed, experiments using mitochondrial membrane potential sensors [21] (rhodamine 123 and MitoTracker) show a reduction of membrane potential following plasma membrane rupture (see Supplemental Figs. 5 and 6). Mitochondrial membrane potential may be modified by ion entry upon plasma membrane rupture. Indeed, membrane potential and mitochondrial fission are sensitive to the intracellular concentration of calcium [22] or potassium [23]. One should also

note that mitochondria associate with the cellular cytoskeleton, which may play a role in the maintenance of the tubular mitochondrial morphology [24]. Our description, however, does not account for this association because there is evidence that mitochondrial morphology is not perturbed by disrupting mitochondrial links to the cell's cytoskeleton [25,26]. Indeed, treatment with pharmacological agents that disrupt the cytoskeleton does not significantly affect either the onset of the instability or the dynamics of shape change (see Supplemental Figs. 2 and 3).

Here we investigate the stability of the tubular mitochondrial shape as a function of the dimensionless number $N_{\mathrm{EC}}$. Unlike Ref. [14], our study not only considers the stability of equilibrium states but also the dynamics of perturbation growth. We consider varicose perturbations [13] and idealize the mitochondrion, which originally has a large aspect ratio (see Fig. 2), as an infinitely long, perturbed cylinder [Fig. 3(a)], whose local radius is given by

$$R = R_0 + \epsilon \exp\{ikz + \sigma t\}. \tag{1}$$

Here, $R_0$ is the undeformed radius of the mitochondrion, $\epsilon \exp\{\sigma t\} \ll R_0$ is the amplitude of the varicose perturbation, $k$ is its wave number, $\sigma$ is the inverse of the characteristic time of growth (if $\sigma > 0$) or decay (if $\sigma < 0$) of the perturbation, $z$ is the longitudinal coordinate along the mitochondrial axis, and $t$ is the elapsed time. In Eq. (1) and in all the complex expressions that follow, it is understood that only the real part is kept on each side of the equations. We perform a linear analysis including terms up to order $\epsilon/R_0$, whereas all higher-order terms are neglected. Mechanically, we describe the mitochondrial matrix as a Newtonian fluid of dynamic viscosity $\mu$, significantly larger than that of water [27,28]. For a typical radius $R_0 \approx 0.1$ $\mu$m and a typical deformation speed $u \approx 0.01$ $\mu$m/s, the Reynolds number of the matrix flow is expected to be $\mathrm{Re} = \rho u R_0/\mu < 10^{-10} \ll 1$. The flow is thus described by the axisymmetric Stokes equations:

$$\frac{\partial p}{\partial r} = \mu\left(\frac{\partial^2 u}{\partial r^2} + \frac{1}{r}\frac{\partial u}{\partial r} - \frac{u}{r^2} + \frac{\partial^2 u}{\partial z^2}\right), \tag{2a}$$

$$\frac{\partial p}{\partial z} = \mu\left(\frac{\partial^2 w}{\partial r^2} + \frac{1}{r}\frac{\partial w}{\partial r} + \frac{\partial^2 w}{\partial z^2}\right), \tag{2b}$$

where $p$ is the pressure relative to the mitochondrial exterior, and $u$ and $w$ are, respectively, the radial ($r$) and longitudinal ($z$) velocity components [see Fig. 3(a)]. The continuity equation reads:

$$\frac{\partial u}{\partial r} + \frac{u}{r} + \frac{\partial w}{\partial z} = 0. \tag{3}$$

The flow field inside the mitochondrion is subjected to the following kinematic boundary conditions at the mitochondrial membrane:

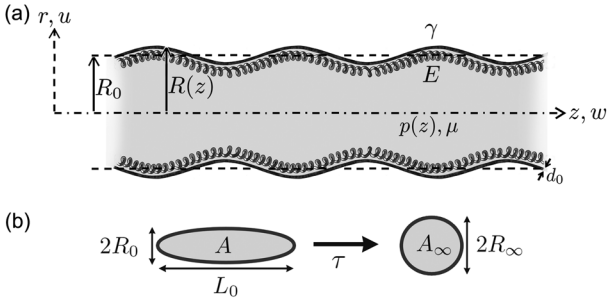



FIG. 3. (a) Conceptualization used in the instability calculation. A mitochondrion is represented by a long cylinder of initial radius $R_0$ with a membrane tension $\gamma$ and elastic modulus $E$, filled with a viscous fluid of viscosity $\mu$. (b) Conceptualization of the shape relaxation process.

$$u(r = R_0) = \frac{\partial R}{\partial t} = \epsilon\sigma \exp\{ikz + \sigma t\}, \tag{4a}$$

$$w(r = R_0) = 0. \tag{4b}$$

The dynamic boundary condition at the mitochondrial membrane is

$$\left(p - 2\mu\frac{\partial u}{\partial r}\right)\bigg|_{r=R} = \gamma\left(\frac{1}{R} - \frac{\partial^2 R}{\partial z^2}\right) + E d_0 \frac{(R - R_0)}{R^2}, \tag{5}$$

where the right-hand side includes a first term representing the capillary force due to membrane tension and a second term representing the elastic force due to mitochondrion stretching [29]. Equation (5) assumes that the membrane bending resistance can be neglected compared to the stretching resistance, which is a reasonable assumption for biological membranes [30]. By solving Equations (2) and (3) subjected to the conditions given by Eqs. (4) and (5) (see the Supplemental Material for mathematical details), we obtain the following dispersion relationship:

$$\sigma = \frac{\gamma}{\mu R_0}[1 - x_0^2 - N_{\mathrm{EC}}] \times \left[\frac{2I_0(x_0)I_1(x_0) - x_0[I_0^2(x_0) - I_1^2(x_0)]}{2x_0[2I_0^2(x_0) - I_1^2(x_0)] - 4I_0(x_0)I_1(x_0)}\right]. \tag{6}$$

The last factor, involving modified Bessel functions of the first kind, is positive for all $x_0 > 0$. Thus, the criterion for instability is $x_0^2 < 1 - N_{\mathrm{EC}}$. Equivalently, instability occurs for wavelengths $\lambda$ such that

$$\lambda > \lambda_{\min} = \frac{2\pi R_0}{\sqrt{1 - N_{\mathrm{EC}}}}. \tag{7}$$

Equation (7) suggests the following explanation of the observed mitochondrial fission: originally, the mitochondrial resistance to deformation is sufficiently large so that elasticity dominates membrane tension and $N_{\mathrm{EC}} > 1$. In this case, Eq. (7) has no real solution and the cylindrical shape of

the mitochondrion is stable. Upon plasma membrane rupture, the mechanical properties of mitochondria are altered and the ratio $E/\gamma$ decreases, so that $N_{EC} < 1$ and the tubular shape becomes unstable. If we suppose that the reduction in $E/\gamma$ is of at least 1 order of magnitude, so that $N_{EC} \approx 0.1$, we deduce $\lambda_{min} \approx 2.1\pi R_0$. It is noted that our results are insensitive to the specific value assumed for $N_{EC}$, as long as it is significantly smaller than 1. Indeed, assuming any other value of $N_{EC} \leq 0.1$ only changes the results by at most 5%. In order to fission into two smaller units, the original mitochondrial length $L_0$ needs to be at least about twice this minimal wavelength; thus, $L_{0,min} \approx 2\lambda_{min} = 4.2\pi R_0$. Figure 4(a) shows that this relationship quite accurately separates experimentally observed stable (nonfissioning) versus unstable (fissioning) mitochondria, as a function of their observed initial radius $R_0$ and length $L_0$. This result offers a mechanical explanation of why the fissioning rate of mitochondria in neurons has been observed to strongly increase with mitochondrial length [31].

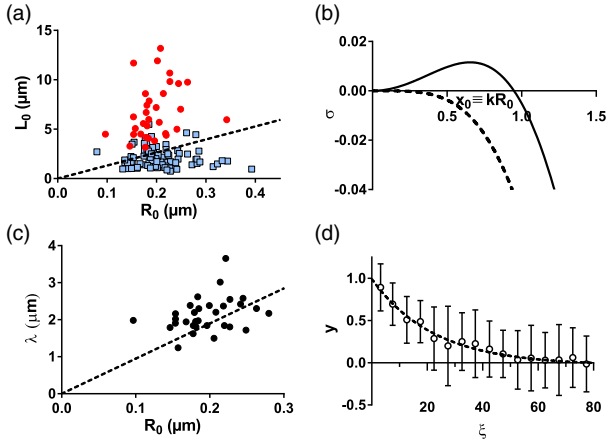



FIG. 4 (color online). (a) Stability phase diagram. Each symbol corresponds to an observed mitochondrion, characterized by its initial radius $R_0$ and its initial length $L_0$. Mitochondrial geometry is determined from the experimental images with an uncertainty of at most 15% due to diffraction blur. Blue squares indicate mitochondria that do not fission upon plasma membrane rupture, and red circles indicate mitochondria that fission into two or more subunits. The dashed line indicates the limit of the stability region predicted by the model $L_0 = 4.2\pi R_0$. (b) Predicted growth rate $\sigma$ for perturbations of different wave number $k$. The solid line is the result of Eq. (6) for $N_{EC} = 0.1$ and the dashed line for $N_{EC} = 1$. (c) Wavelength $\lambda$ of the observed instability, as a function of the mitochondrial initial radius $R_0$. Circles correspond to experimental measurements, and the dashed line corresponds to the model's prediction $\lambda \approx 9.5R_0$. (d) Evolution of the mitochondrial shape as a function of the elapsed time. The figure represents the normalized time $\xi \equiv t/\tau$ versus the normalized projected area $y \equiv [(A-A_\infty)/(A+A_\infty)][(A_0+A_\infty)/(A_0-A_\infty)]$. The symbols represent the mean and the standard deviation of the measurements. (We followed 29 mitochondria belonging to three different cells.) The dashed line represents the fit of Eq. (9), with a value of the fitting parameter $\gamma/\mu = 0.045$ $\mu$m/s.

Figure 4(b) shows the dependence of $\sigma$ on $x_0 \equiv kR_0$ given by Eq. (6) for a stable condition $N_{EC} = 1$ (dashed line) and for an unstable condition $N_{EC} = 0.1$ (solid line). The maximum of the solid line is reached at $x_0 = 0.66$ and $\sigma = 0.012\gamma/(\mu R_0)$. This result implies that, for fissioning mitochondria, the typical length of the instability is expected to be $\lambda = 2\pi R_0/x_0 \approx 9.5R_0$. This prediction is in close agreement with the typical mitochondrial fragment size that we observe experimentally just after fission, as shown in Fig. 4(c), as well as with observations reported in the literature that neural mitochondria longer than about 3 $\mu$m have a significantly increased probability of undergoing fission [31].

Once the tubular shape has become unstable, the evolution dynamics of the mitochondrial fragments towards their final spheroidal shape is a nonlinear phenomenon. Here we propose a simple description of these dynamics using scaling arguments. Mitochondrial shape relaxation [Fig. 3(b)] is governed by a balance between membrane tension, which tends to round mitochondria, and viscous dissipation, which resists deformation. The mitochondrial surface energy can be written as $\mathcal{E} = \gamma S \approx 4\gamma A$, where $S$ is the mitochondrial surface area and $A$ is the projected surface area as visualized in a microscope image. By scaling the velocity gradient as $|\nabla \mathbf{u}| \sim (-dL/dt)/(L/2 - R_\infty)$, which is approximated as a constant over the mitochondrial volume, the viscous energy dissipation can be approximated by

$$\frac{d\mathcal{E}}{dt} = -\mu \int_V \nabla \mathbf{u} : \nabla \mathbf{u}\, dV \sim -\pi\mu \frac{R^2}{L/2 - R_\infty}\left(-\frac{dL}{dt}\right)^2, \quad (8)$$

where $R$ and $L$ are the radius and length of the mitochondrial fragment at time $t$, and $R_\infty$ is the final radius of the mitochondrial fragment once it has reached its final shape [see Fig. 3(b)]. To simplify the above expression, the total mitochondrial volume has been approximated by $\pi R^2(L - 2R_\infty)$ when performing the integral. It is noted that elastic effects are neglected in Eq. (8). This is consistent with the necessary condition for the instability to arise $N_{EC} < 1$, implying that surface tension effects dominate elasticity. Assuming that the mitochondrial fragment is ellipsoidal, conservation of volume requires that $2\pi R^2 L/3 = 2\pi R_0^2 L_0/3 = 4\pi R_\infty^3/3$, where $R_0$ and $L_0$ are the initial radius and length of the mitochondrial fragment. Therefore, $R_\infty = (R_0^2 L_0/2)^{1/3}$. Conservation of volume together with Eq. (8) yields

$$\left(\frac{A - A_\infty}{A + A_\infty}\right) = \left(\frac{A_0 - A_\infty}{A_0 + A_\infty}\right) e^{-t/\tau}, \quad (9)$$

where $A_\infty = \pi R_\infty^2 = \pi(R_0^2 L_0/2)^{2/3}$ is the final projected surface area of the mitochondrion, and $\tau = \mu R_\infty/(2\gamma)$ is the characteristic shape relaxation time. Figure 4(d) shows the experimentally observed evolution of the mitochondrial

area, normalized according to the scaling suggested by Eq. (9). Normalized values for different mitochondria are well fitted by the theoretical prediction, with the only fitting parameter being $\gamma/\mu = 0.045$ $\mu$m/s. This value corresponds to a typical time for shape relaxation of $\tau \sim 10$ s.

We can use our results to infer estimates of the mitochondrial mechanical properties. A previous study of micropipette aspiration of isolated mitochondria reported a mitochondrial membrane tension of the order of $\gamma \approx 10^{-5}$ N/m [16]. This together with our measurement of $\gamma/\mu$ yields an estimate of the mitochondrial viscosity of $\mu \approx 200$ Pa s, which is of the same order of magnitude as the typical viscosity of a whole cell [32]. If we assume $N_{EC} \approx 1$ and a double-membrane thickness $d_0 \approx 10$ nm, we deduce $E \approx 10^3$ Pa. Indeed, mitochondria aspirated into a micropipette deform over a typical time of about 200 ms [16], which matches our estimate of $\mu/E$, the characteristic time of deformation of a viscoelastic body.

In conclusion, our results strongly suggest that mechanical phenomena play an important role in regulating mitochondrial morphology. A change in the mitochondrial mechanical properties, for example, due to a reduction in the effective elastic modulus, suffices to initiate fission of a mitochondrion into smaller fragments. Once the mechanical perturbation occurs, mitochondrial fission and rounding occur spontaneously, without the need for further intervention by auxiliary proteins. The mechanical instability we have described explains the biological observation that the occurrence of fission is dependent on mitochondrial length, as longer mitochondria become unstable more readily upon a mechanical perturbation.

This work was partially supported by a permanent endowment in cardiovascular cellular engineering from the AXA Research Fund. D. T. is funded by the AFM Trampoline (Grant No. 16799).

*davidgr@alum.mit.edu
Present address: Institut de Chimie, Physique et Matériaux, Université de Lorraine, 57078 Metz, France.
†julien.husson@ladhyx.polytechnique.fr

[1] C. S. Palmer, L. D. Osellame, D. Stojanovski, and M. T. Ryan, Cellular signalling **23**, 1534 (2011).
[2] L. M. Westrate, J. A. Drocco, K. R. Martin, W. S. Hlavacek, and J. P. MacKeigan, PLoS One **9**, e95265 (2014).
[3] B. Westermann, Nat. Rev. Mol. Cell Biol. **11**, 872 (2010).
[4] D. Arnoult, Trends Cell Biol. **17**, 6 (2007).
[5] F. Stavru, F. Bouillard, A. Sartori, D. Ricquier, and P. Cossart, Proc. Natl. Acad. Sci. U.S.A. **108**, 3612 (2011).
[6] F. Stavru, A. E. Palmer, C. Wang, R. J. Youle, and P. Cossart, Proc. Natl. Acad. Sci. U.S.A. **110**, 16003 (2013).
[7] See Supplemental Material at http://link.aps.org/supplemental/10.1103/PhysRevLett.115.088102, which includes Refs. [8–11], for details on the mathematical derivation, on the experimental protocol, and on the molecular mechanisms underlying the observed morphological change.
[8] A. Edelstein, N. Amodaj, K. Hoover, R. Vale, and N. Stuurman, Curr. Protoc. Mol. Biol. **92**, 14.20.1 (2010).
[9] W. Pendergrass, N. Wolf, and M. Poot, Cytometry **61A**, 162 (2004).
[10] K. Gilmore and M. Wilson, Cytometry **36**, 355 (1999).
[11] C. Cottet-Rousselle, X. Ronot, X. Leverve, and J.-F. Mayol, Cytometry **79A**, 405 (2011).
[12] J. Plateau, *Statique Expérimentale et Théorique des Liquides Soumis aux Seules Forces Moléculaires* (Gauthier-Villars, Paris, 1873).
[13] J. W. S. Rayleigh, Proc. London Math. Soc. **s1-10**, 4 (1878).
[14] R. Bar-Ziv and E. Moses, Phys. Rev. Lett. **73**, 1392 (1994).
[15] E. Hannezo, J. Prost, and J.-F. Joanny, Phys. Rev. Lett. **109**, 018101 (2012).
[16] S. Wang, C. Jiang, Y. Zhang, J. Chen, B. Wang, Q. Chen, and M. Long, Cell. Mol. Bioeng. **1**, 67 (2008).
[17] C. A. Mannella, D. R. Pfeiffer, P. C. Bradshaw, I. I. Moraru, B. Slepchenko, L. M. Loew, C. Hsieh, K. Buttle, and M. Marko, IUBMB Life **52**, 93 (2001).
[18] S. Jung, C. Clanet, and J. W. M. Bush, Soft Matter **10**, 3225 (2014).
[19] E. Gottlieb, S. M. Armour, M. H. Harris, and C. B. Thompson, Cell Death Differ. **10**, 709 (2003).
[20] M. Chvanov, J. Phys. Chem. B **110**, 22903 (2006).
[21] L. B. Chen, Annual Review of Cell Biology **4**, 155 (1988).
[22] D. V. Jeyaraju, G. Cisbani, and L. Pellegrini, Biochim. Biophys. Acta **1787**, 1363 (2009).
[23] K. S. Dimmer, F. Navoni, A. Casarin, E. Trevisson, S. Endele, A. Winterpacht, L. Salviati, and L. Scorrano, Human Molecular Genetics **17**, 201 (2008).
[24] I. R. Boldogh and L. A. Pon, Biochim. Biophys. Acta **1763**, 450 (2006).
[25] L. Griparic and A. M. van der Bliek, Traffic **2**, 235 (2001).
[26] Y. Shibata, J. Hu, M. M. Kozlov, and T. A. Rapoport, Annu. Rev. Cell Dev. Biol. **25**, 329 (2009).
[27] B. A. Scalettar, J. R. Abney, and C. R. Hackenbrock, Proc. Natl. Acad. Sci. U.S.A. **88**, 8057 (1991).
[28] Z. Yang, Y. He, J.-H. Lee, N. Park, M. Suh, W.-S. Chae, J. Cao, X. Peng, H. Jung, C. Kang, and J. S. Kim, J. Am. Chem. Soc. **135**, 9181 (2013).
[29] V. Duclaux, F. Gallaire, and C. Clanet, J. Fluid Mech. **664**, 5 (2010).
[30] R. Philips, J. Kondev, and J. Theriot, *Physical Biology of the Cell* (Garland, New York, 2009).
[31] M. Cagalinec, D. Safiulina, M. Liiv, J. Liiv, V. Choubey, P. Wareski, V. Veksler, and A. Kaasik, J. Cell Sci. **126**, 2187 (2013).
[32] R. M. Hochmuth, J. Biomech. **33**, 15 (2000).